JOURNAL OF THEORETICAL AND APPLIED MECHANICS
61, 2, pp.395-406, Warsaw 2023
https://doi.org/10.15632/jtam-pl/161686

A FULLY-COUPLED THREE-DIMENSIONAL FLUID-STRUCTURE INTERACTION STUDY ON THE EXTERNALLY-PRESSURIZED COLLAPSIBLE TUBE AND THE INTERNAL FLOW

Sen Zhang
Department of Mechanics and Engineering Science, College of Engineering, Peking University, Beijing, China; and Beijing Internet Based Engineering Co., Ltd, Beijing, China
e-mail: tjuzhangsen@163.com

HaoFei Liu
Department of Mechanics, Tianjin University, Tianjin, China
e-mail: hfliu@tju.edu.cn

We study the behavior of a collapsible tube conveying a fluid subject to external pressure that could occur in many physiological applications. The method of rotating spines is developed to enable an automatic mesh adaptation when the tube is deformed largely. We examine bifurcation diagrams when the tube is collapsed under a pressure driven condition and reveal that multiple solutions exist for a range of the Reynolds number. The stability characteristic of the system is discovered by determining stability of these solutions by the eigenvalue method for the first time, which is validated by solving a time-dependent problem of the system.

Keywords: fluid structure interaction, stability, eigenvalue problem, bifurcation

1. Introduction

The flow in collapsible tubes has been widely studied for its numerous applications to physiology and medical devices in the last few decades. An intriguing feature of this system is the flow-induced self-excited oscillation. Physiological examples include respiratory wheezes during forced expiration, cervical venous hum arising through oscillations of the external jugular vein, generation of snoring noises, the Korotkoff sounds heard when the blood pressure is measured by applying an external force on an artery. We refer readers to (Heil and Jensen, 2003; Grotberg and Jensen, 2004) for a more detailed discussion of physiological applications of collapsible tube flows.

Self-excited oscillations are frequently observed in a laboratory in the "Starling resistor". Early experiments on collapsible tubes tended to investigate classification of different oscillations, influence of different system parameters on the oscillation and analyzed pressure, flow rate and tube cross-sectional area time records in many test cases (Bertram, 2003). However, flow characteristics within the tube when it is in a state of self-oscillation are lacking. This is because invasive experimental techniques measuring pressure and velocity have a great effect on the flow field. Much recent experimental work has concentrated on visualization of the flow fields using high speed particle image velocimetry. The time-varying flow field just downstream of an oscillating collapsible tube was measured by Bertram *et al.* (2008). Truong and Bertram (2009) measured the flow-field immediately downstream of a collapsible tube during oscillation onset starting from the collapsed state and identified the areas of the flow where oscillation initially occurred. The velocity fields in the flexible tube when it is on the verge of the self-oscillation state and is in the state of periodic self-oscillation has been measured (Yiasemides *et al.*, 2017).

To understand the mechanisms of self-excited oscillations of the system observed, many researchers use a two-dimensional channel in which a part of one of the sidewalls is replaced by a pre-stressed elastic membrane or a tube. When the prestress is small, the viscous pressure drop along the channel induces large-amplitude and low-frequency self-excited oscillations. Luo *et al.* (2008) analyzed the system linear stability in the absence of prestress and discovered a "cascade" stability structure for the flow-driven boundary condition (the fluid velocity is imposed at the inlet). Liu *et al.* (2012) found different oscillation modes when the system was pressure-driven (the fluid press was imposed at the inlet). Jensen and Heil (2003) employed asymptotic techniques to derive explicit predictions for stability boundaries for small-amplitude, high-frequency, self-excited oscillations in the limit of large membrane tension and identified a simple sloshing mechanism for self-excited oscillations. In three dimensions, Heil and Boyle (2010) found the sloshing mechanism which explained the development of self-excited oscillation in initially axisymmetric (or weakly buckled) three-dimensional collapsible tubes. Zhang *et al.* (2018) examined bifurcation diagrams for different collapse models in the velocity driven condition and revealed that multiple solutions exist in some range of the Reynolds number. Although Whittaker *et al.* (2010) predicted the onset of high-frequency self-excited oscillations by considering energy budget of the system, and analyzed stability of the system by direct numerical simulation which had not been done before.

In this paper, we investigate a flow-tube system in the pressure driven condition based on the model developed by Zhang *et al.* (2018). An outline of the paper is as follows. In Section 2, we introduce the model briefly. In Section 3, several methods are introduced to solve the problem including the finite element method and the eigenvalue method. In the finite element method, improved three-dimensional rotating spines are used to update the adaptive mesh deformation. In Section 4, the steady flow-tube system is solved under different pressures in a range of Reynolds numbers in the pressure driven condition, and the system buckling behavior is studied for different Reynolds numbers. The stability of some solutions is also identified by the eigenvalue method which is validated by solving the transient solution of the system. In Section 5, conclusions are included and some further researches are discussed.

2. The fluid-tube model

2.1. Model description

The model consists of a flow in a three-dimensional collapsible tube whose cross section is cylindrical initially. The tube has a thickness h^*, length L^* and inner diameter D^*. We divide the tube into the upstream part, middle part and downstream part with the length L_u^*, L_m^* and L_d^*, respectively. The upstream and downstream parts are rigid and the middle part which is subjected to an external pressure P_{ext}^* and is assumed to be collapsible as shown in Fig. 1. The tube is described by a neo-Hookean material with the density ρ_e^* and shear modulus μ_e^*. The fluid is an incompressible Newtonian fluid whose density is ρ^* and viscosity is μ^*. The flow is assumed to be laminar and the average flow velocity of the tube is U_0^*.

2.2. The governing equations

The governing equations are built by the ALE method. The fluid governing equations are built in the Eulerian coordinate system with the position vector $\mathbf{x}$, and the solid governing equations are built in two Lagrangian coordinate systems using $\mathbf{x}_e$ and $\mathbf{X}_e$, respectively. $\mathbf{x}_e$ is the position vector in the current configuration and $\mathbf{X}_e$ is the position vector in the reference configuration.

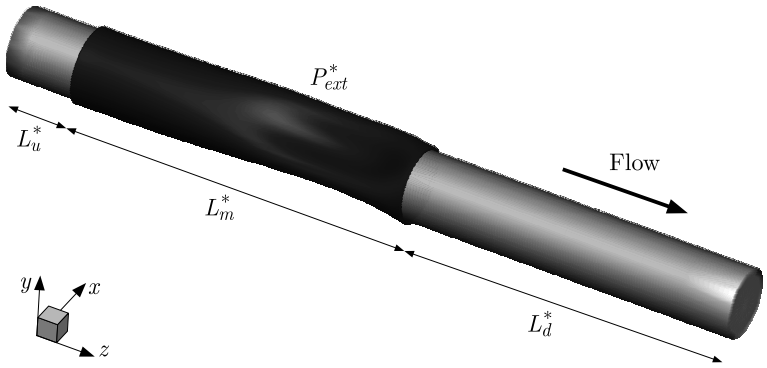

Fig. 1. Geometry of the collapsible tube

For convenience, we adopt dimensionless variables and parameters defined as follows,

$$
\begin{aligned}
&x_i = \frac{x_i^*}{D^*} \qquad x_{ei} = \frac{x_{ei}^*}{D^*} \qquad X_{ei} = \frac{X_{ei}^*}{D^*} \qquad i = 1,2,3\\
&v_i = \frac{v_i^*}{U_0^*} \qquad u_i = \frac{u_i^*}{D^*} \qquad i = 1,2,3\\
&L_u = \frac{L_u^*}{D^*} \qquad L_m = \frac{L_m^*}{D^*} \qquad L_d = \frac{L_d^*}{D^*} \qquad L = \frac{L^*}{D^*}\\
&h = \frac{h^*}{D^*} \qquad \rho_e = \frac{\rho_e^*}{D^*}\rho^* \qquad t = \frac{D^* t^*}{U_0^*}\\
&p = \frac{p^*}{\rho^* U_0^{*2}} \qquad P_{ext} = \frac{P_{ext}^*}{\rho^* U_0^{*2}} \qquad \mathrm{Re} = \frac{U_0^* D^* \rho^*}{\mu^*} \qquad \mu_e = \frac{\mu_e^*}{\rho^* U_0^{*2}}
\end{aligned}
\tag{2.1}
$$

where the quantities with a star are dimensional ones. v_i, x_i $(i = 1,2,3)$ are velocity and coordinate components of the fluid, u_i $(i = 1,2,3)$ are displacement components of the structure, and x_{ei}, X_{ei} $(i = 1,2,3)$ are coordinate components of the structure in the current and reference configuration, respectively. P is the fluid pressure, Re is the Reynolds number.

The dimensionless governing equations for the coupled fluid-structure interaction system are

$$
\begin{aligned}
&\frac{\partial v_i}{\partial t} + v_j \frac{\partial v_i}{\partial x_j} = -\frac{\partial p}{\partial x_i} + \frac{1}{\mathrm{Re}} \nabla^2 v_i\\
&\frac{\partial v_i}{\partial x_i} = 0 \qquad \det \mathbf{F} = 1\\
&\mu_e F_{iA,A} - p_e F^{-1}_{Ai,A} = \rho_e u_{i,tt} \qquad i,j,A = 1,2,3
\end{aligned}
\tag{2.2}
$$

where $\mathbf{F}$ is the deformation gradient.

2.3. The boundary conditions

We impose the following boundary conditions:

1) Parallel, axially traction-free inlet flow ($z = 0$): $v_1 = v_2 = P = 0$.
2) Zero velocity at the rigid walls ($r = R$, $0 \leqslant z \leqslant L_u$, $L_u + L_m \leqslant z \leqslant L$): $v_i = 0$, $i = 1,2,3$.
3) Parallel flow with the required flow rate at the outflow ($z = L$): $v_1 = v_2 = 0$; $\int v_3 \, dA = \pi/4$.
4) Clamped ends of the elastic tube ($z = L_u$, $L_u + L_m$): $u_i = 0$, $\dot{u}_i(t) = 0$, $i = 1,2,3$.
5) No slip condition at the interface ($L_u \leqslant z \leqslant L_u + L_m$, $r = R$): $v_i(t) = \dot{u}_i(t)$, $i = 1,2,3$.
6) External pressure on the outer wall of the tube: $\boldsymbol{\sigma} \times \mathbf{n} = -P_{ext}\mathbf{n}$, where $\mathbf{n}$ is the outward normal vector of the tube.

3. The numerical method

3.1. The adapting mesh

The finite-element method is adopted to solve the coupled nonlinear fluid-structure interactive equations simultaneously, and the method of rotating spines is used to enable an automatic mesh adaptation. To construct the adapting mesh, we once divided the fluid field in the elastic section into internal and external regions by a virtual cylindrical shell. The nodes within the cylindrical shell are fixed, and these outside the shell are movable. The spines are originating from the virtual cylindrical shell. The deformed by this method mesh is shown in Fig. 2. It can be seen when the deformation is large, the mesh in the internal section is denser than the mesh in the external section. It goes against the law that density of the mesh towards the wall should be increased to resolve the boundary layer near the tube wall.

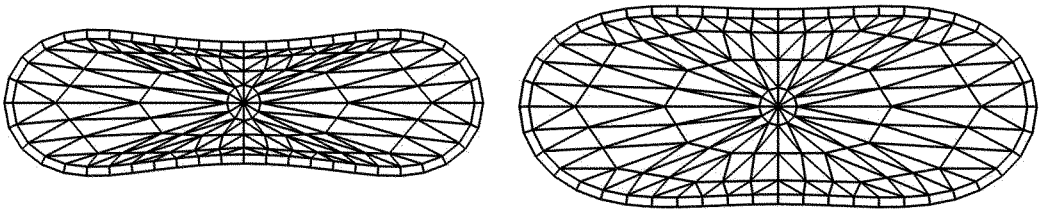

Fig. 2. The deformed mesh by the prior method

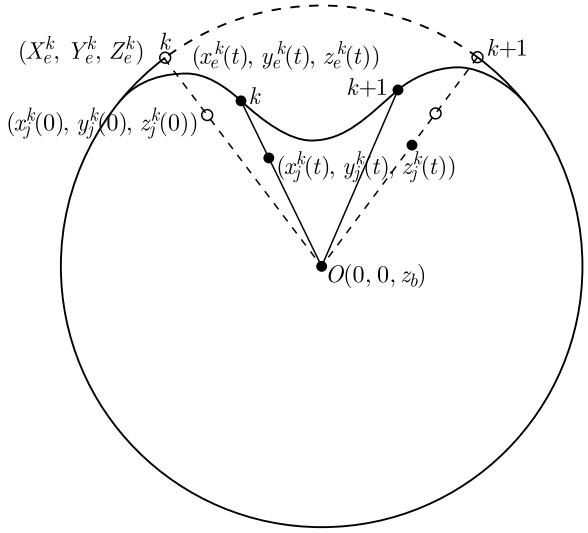

Fig. 3. A sketch of the moving rotating spines

We improve the method by cancelling the cylindrical shell and the spines originating from the center line of the tube. This method is illustrated on a circular cross section as shown in Fig. 3. The spines are straight lines which can rotate around the fixed node in the center. For example, $(x_j^k(0), y_j^k(0), z_j^k(0))$ are the initial coordinates of the (fluid) node j on the spine k which is connecting the fixed node $O(0,0,z_b)$ in the center to the material point (X_e^k, Y_e^k, Z_e^k) on the tube wall. After deformation, (X_e^k, Y_e^k, Z_e^k) moves to $(x_e^k(t), y_e^k(t), z_e^k(t))$ according to

$$x_e^k(t) = X_e^k + u_e(t) \qquad y_e^k(t) = Y_e^k + v_e(t) \qquad z_e^k(t) = Z_e^k + w_e(t) \tag{3.1}$$

where (u_e, v_e, w_e) are the corresponding displacements. The node $(x_j^k(0), y_j^k(0), z_j^k(0))$ on the spine k moves along it according to

$$x_j^k(t) = \omega_j^k x_e^k(t) \qquad y_j^k(t) = \omega_j^k y_e^k(t) \qquad z_j^k(t) = z_b^k + \omega_j^k (z_e^k(t) - z_b) \tag{3.2}$$

where $j = 1, 2, 3, \ldots, n_k$, n_k is the total number of nodes on the spine k, and ω_j^k are the fixed scaling factors defined by

$$\omega_j^k = \frac{\sqrt{(x_j^k(0))^2 + (y_j^k(0))^2 + (z_j^k(0) - z_b)^2}}{\sqrt{(X_e^k)^2 + (Y_e^k)^2 + (Z_e^k - z_b)^2}} \tag{3.3}$$

After we obtain the coordinates of the nodes on the rotating spines, those which are not placed on the rotating lines are linearly interpolated from those on the rotating spines. The deformed mesh by the new method is shown in Fig. 4.

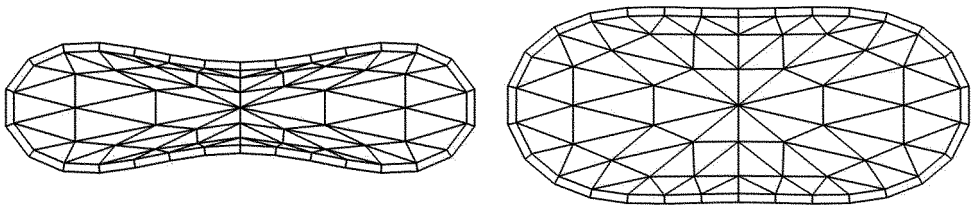

Fig. 4. The deformed mesh by the new method

3.2. Fully coupled finite-element equations

When solving the time-dependent problem, the time derivatives in the finite element equations need to be replaced by the finite time difference terms. In the solid equations, the acceleration term is expressed by the second-order partial derivative of displacement with respect to time. But it is expressed by the one-order partial derivative of velocity with respect to time in the fluid equations. In order to adopt the same time difference scheme to approximate the acceleration term, we unify the order of partial derivative with respect to time by adding the variables of solid velocity. The relationship between velocities of the solid and its displacements is

$$u_{i,t} = \alpha_i \qquad i = 1, 2, 3 \tag{3.4}$$

where α_i is the solid velocity in the x, y, z directions.

We employ the Petrov-Galerkin method to discretize governing equations (2.2). To make the order of each item in the discretization equations be the same, the element type for the flow is a 15 node triangular prism with quadratic shape functions ψ for velocities and linear shape functions φ for fluid pressure. The element type for the solid is a 20 node hexahedron with quadratic shape functions ψ^e for displacements, solid velocities and linear shape functions φ^e for the solid 'pressure'.

Coupled governing equations (2.2) when they are discretized and assembled, can be written in a matrix form as

$$\mathbf{M}\frac{d\mathbf{U}}{dt} + \mathbf{K}(\mathbf{U})\mathbf{U} - \mathbf{F}' = \mathbf{R} = \mathbf{0} \tag{3.5}$$

where $\mathbf{U} = [u_j, v_j, w_j, p_j, u_{ej}, v_{ej}, w_{ej}, p_{ej}, \alpha_{xj}, \alpha_{yj}, \alpha_{zj}]^{\mathrm{T}}$ is the global vector of unknowns, j is the number of degrees of freedom for each variable. $\mathbf{M}$, $\mathbf{K}$ are the $n \times n$ mass and stiffness matrices, respectively. $\mathbf{F}'$ and $\mathbf{R}$ is a force-like vector and residual vector with dimension n, respectively. n is the total number of degrees of freedom. $\mathbf{R}$ is denoted by

$$\mathbf{R} = [R_u, R_v, R_w, R_p, R_{u_e}, R_{v_e}, R_{w_e}, R_{p_e}, R_{\alpha_x}, R_{\alpha_y}, R_{\alpha_z}]^{\mathrm{T}} \tag{3.6}$$

where the subscripts u, v, w, p indicate the corresponding residuals of flow momentum equations in the x, y, z directions and continuity equation, respectively. Subscripts u_e, v_e, w_e, p_e indicate

the corresponding residuals of solid momentum equations and the incompressible equation. Subscripts α_x, α_y, α_z indicate the corresponding residuals of equation (3.4).

When we consider the quasi-static wall and steady flows only, the terms related to time disappear. The coupled governing equations become

$$\mathbf{K}(\mathbf{U})\mathbf{U} - \mathbf{F}' = \mathbf{R} = \mathbf{0} \tag{3.7}$$

where $\mathbf{U} = [u_j, v_j, w_j, p_j, u_{ej}, v_{ej}, w_{ej}, p_{ej}]^{\mathrm{T}}$ is the global vector of unknowns.

3.3. The stability analysis

The system shows different unsteady behavior under different parameters. To study stability of the system, there are usually two methods. One is solving the eigenvalue problem of the system, the other is solving the time-dependent problem of the system. The similarity between the two methods is that the steady solution denoted by $\overline{\mathbf{U}}$ is obtained for a given set of parameters first. The steady solution satisfies the equation

$$\mathbf{K}\overline{\mathbf{U}}\overline{\mathbf{U}} - \mathbf{F}' = \mathbf{0} \tag{3.8}$$

which is solved by the frontal method and the Newton Raphson scheme.

For the method of solving the time-dependent problem, a slightly different steady solution is used as the initial guess which has a parameter value of P_{ext}, say, 1% away from that of the steady solution in question. An implicit finite-difference second order predictor corrector scheme with a variable time step is used to deal with time derivatives (Gresho *et al.*, 1980). After doing this, the time-dependent problem can be solved as the steady problem at each time step. If as time progresses, the time-dependent solution converges to the corresponding steady solution, then the system is stable under the set of parameters. If the time-dependent solution diverges away from the steady solution or oscillates with time, it is deemed to be unstable. The critical point at which the system becomes unstable is called the neutrally stable point.

When solving the eigenvalue problem of the system, an infinitesimal perturbation denoted by $\Delta\mathbf{U}$ is applied to the steady solution. The perturbation can be written as $\Delta\mathbf{U} = \exp(\omega t)(\mathbf{U})$, where $\omega = (\omega_R + \mathrm{i}\omega_I)$ and $\overline{\mathbf{U}} = (\overline{\mathbf{U}}_R + \mathrm{i}\overline{\mathbf{U}}_I)$ are the complex eigenvalues and eigenvectors, respectively. The solution of the system can be expressed as $\mathbf{U} = \overline{\mathbf{U}} + \Delta\mathbf{U}$. We then substitute this formula into discretized matrix equation (3.5). By using of the Taylor expansion and equation (3.8), we obtain a generalized eigenvalue problem

$$\omega\overline{\mathbf{M}}\widetilde{\mathbf{U}} + \overline{\mathbf{K}}\widetilde{\mathbf{U}} = \mathbf{0} \tag{3.9}$$

where $\overline{\mathbf{M}} = \mathbf{M}(\overline{\mathbf{U}})$ and $\overline{\mathbf{K}} = \mathbf{K}(\overline{\mathbf{U}}) + \nabla_{\mathbf{U}}\mathbf{K}(\mathbf{U})|_{\overline{\mathbf{U}}}\overline{\mathbf{U}}$. They can be determined by the steady solution $\overline{\mathbf{U}}$. The above eigenvalue problem is then solved using the ARPACK(https://www.caam.rice.edu/software) software. The Arnold-frontal method employing a frontal method during along with the Arnold iteration scheme is used, for details see (Hao *et al.*, 2016). The advantage of this method is that it just needs to solve the leading few eigenvalues of the discretized system and it does not need to form large matrices $\overline{\mathbf{M}}$ and $\overline{\mathbf{K}}$ in equation (3.9). The stability of the system is decided by the signs of ω_R. If ω_R is positive, the system is unstable and if ω_R is negative, the system is stable. $\omega_R = 0$ indicates the system is at a neutral stable point, which is associated with sustained self-excited oscillations.

The eigenvalue method is adopted in the paper to study stability of the system. It is more effective than the method of solving the time-dependent problem which is used as the validation method of the eigenvalue approach.

4. Results

4.1. The bifurcation diagrams

We study the changes of the system buckling behavior due to changes in the flow rate or the Reynolds number under different external pressures. The geometrical parameters of the model are as follows

$$D^* = 0.004\,\mathrm{m} \qquad L_u = 0.5 \qquad L_m = 10.0 \qquad L_d = 4.0 \qquad h = 0.025$$

The results are presented in terms of the dimensional shear modulus and pressure, i.e. $\mu_e^* = 612000.0$ Pa, external pressures $\mu_e^* = 19.36$ Pa, 19.39 Pa, 19.48 Pa and a pressure drop dp^* across the tube between $z = 0$ and 14.5.

The Reynolds numbers are varied from 40 to 210, the relationship between the Reynolds number and the pressure drop dp^* is shown in Fig. 5 for different values of the external pressure. The straight lines are obtained for axisymmetric deformation, and these remain almost the same under different external pressures. Because the cross-section of the tube keeps to be circular for axisymmetric deformation and the deformation is also small. In this condition, the pressure drop can be obtained by the following formula

$$dp^* = \frac{32L^*\mu^{*2}}{\rho^* D^{*3}}\mathrm{Re} \tag{4.1}$$

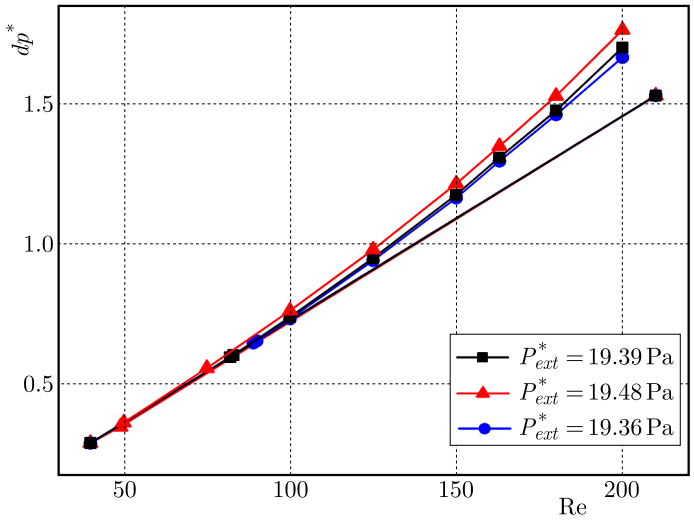

Fig. 5. The relation between Re and dp^* under different external pressures

It is linear with the Reynolds number. The other lines are obtained when the tube is collapsed. The number of pressure drops is equal to the number of solutions of the system. Take the external pressures $P_{ext}^* = 19.36$ Pa as an example, when the Reynolds number is small, just one axisymmetric solution exists. As Re increases to Re > 89, there are two solutions: one axisymmetric and one buckling. This trend is the same for $P_{ext}^* = 19.39$ Pa and 19.48 Pa except for the critical Re $= 82$ and 49, respectively. It can be seen that the critical Reynolds number is decreased as the external pressure increases. Because the tube buckles when the transport pressure (the external pressure minus the internal pressure) exceeds the critical buckling value. When the inlet pressure is imposed, the large external pressure may make the transport pressure arrive at the critical buckling value when the Reynolds number is small according to Eq. (4.1). In the pressure driven boundary condition, the number of solutions is much different with that

under the flow-driven boundary condition in which the system may have one axisymmetric solution, one axisymmetric solution with one buckling solution or two buckling solutions.

To analyse the tube deformation under different Reynolds numbers, we choose point P_2 and point Q_2 which is the intersection point of cut1 and cut2 with the cross section at $z - L_u = 5.0$, respectively, as the characteristic point shown in Fig. 6a. We can also plot a bifurcation diagram in terms of tube deformation and Re by these two points as shown in Fig. 6b. The vertical axis shows the difference of r_0 and r, where r_0 is radius of the tube and r is the distance between the characteristic point and the center of the cross section after deformation. The three overlapped straight lines are obtained when the tube is deformed symmetrically. The lines above the straight lines indicate the wall bulged out at point P_2, and the blow ones indicate the wall collapse at point Q_2. We take $P^*_{ext} = 19.48\,\text{Pa}$ as an example to show the tube deformation when Re increases. When Re is less than the critical Re, which is 49 in this situation, the tube deformation is symmetrical and small, and increases slowly as Re increases. At the critical point, the tube may buckle and the symmetrical deformation disappears. The deformation of the tube will increase rapidly as Re increases if it is on the buckling branch.

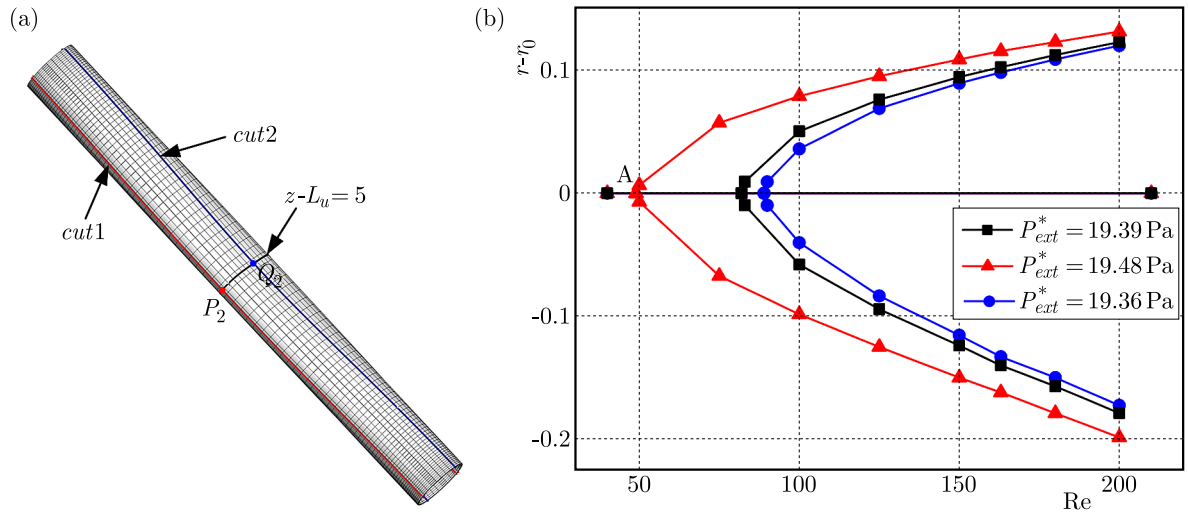

Fig. 6. (a) The sketch of the positions of characteristic points and (b) the buckling curves of the characteristic points under different external pressures

4.2. Stability analysis of the system

We investigate stability of the steady solutions obtained in Section 4.1 by the eigenvalue method described in Section 3.3. The axisymmetric deformation of the tube is small and the most likely to occur. So, the steady solution when the tube is axisymmetric is stable normally, we also validate this in some cases. We focus the attention on the buckling solutions next.

The eigenvalues of the stability problem of buckling solutions with different Re under three different external pressures when the system is in pressure driven condition are shown in Table 1. It shows that as the external pressure increases, the real part of the eigenvalue becomes smaller and smaller at the same Re. Take Re = 180 as an example, when $P^*_{ext} = 19.39\,\text{Pa}$, then the real part of the eigenvalue is 0.0096. As the external pressure increases to 19.39 Pa and 19.48 Pa, the real part of the eigenvalue decreases to 0.0086 and −0.00050, respectively. The stability of the steady solution becomes unstable from stable. It can be inferred that with an increase of external pressure, the buckling solution changes from an unstable solution to a stable one when other parameters remain unchanged. The table also shows that the real part of the eigenvalue becomes larger and larger with an increase of Re at the same external pressure. Take $P^*_{ext} = 19.36\,\text{Pa}$ as an example, when Re = 125, the real part of the eigenvalue is −0.014. As the Re increases to

150 and 163, the real part of the eigenvalue increases to −0.000203 and 0.0057, respectively. It can be observed that there is a critical Re where the real part of the eigenvalue is zero between the 150 and 163. The buckling solution with the Re below the critical Re is stable, and above the critical Re is unstable. At external pressure $P^*_{ext} = 19.39\,\text{Pa}$, the critical Re is between 150 and 163. When the external pressure $P^*_{ext} = 19.48\,\text{Pa}$, it can be considered that the critical Re is 200. Although the real part of the eigenvalue is not exactly equal to zero, considering the error of the numerical method, the real part of the eigenvalue can be approximated to zero.

Table 1. Eigenvalues of stability problem of buckling solutions with different Re under three different external pressures when the system is in the pressure driven condition

Re	$P^*_{ext} = 19.36\,\text{Pa}$		$P^*_{ext} = 19.39\,\text{Pa}$		$P^*_{ext} = 19.48\,\text{Pa}$	
	Real	Imaginary	Real	Imaginary	Real	Imaginary
125	−0.014	0.625	−0.018	0.676	−0.024	0.714
150	−0.000203	0.582	−0.00201	0.584	−0.00816	0.634
163	0.0057	0.524	0.0035	0.542	−0.00502	0.583
180	0.0096	0.486	0.0086	0.487	−0.00050	0.524
200	0.0119	0.436	0.0099	0.446	0.000091	0.476

4.3. Validation of stability of the system

In this Section, the stability of the steady-state solution is determined by solving the transient solution of the system, and the results are compared with those obtained by the eigenvalue method in Section 4.2.

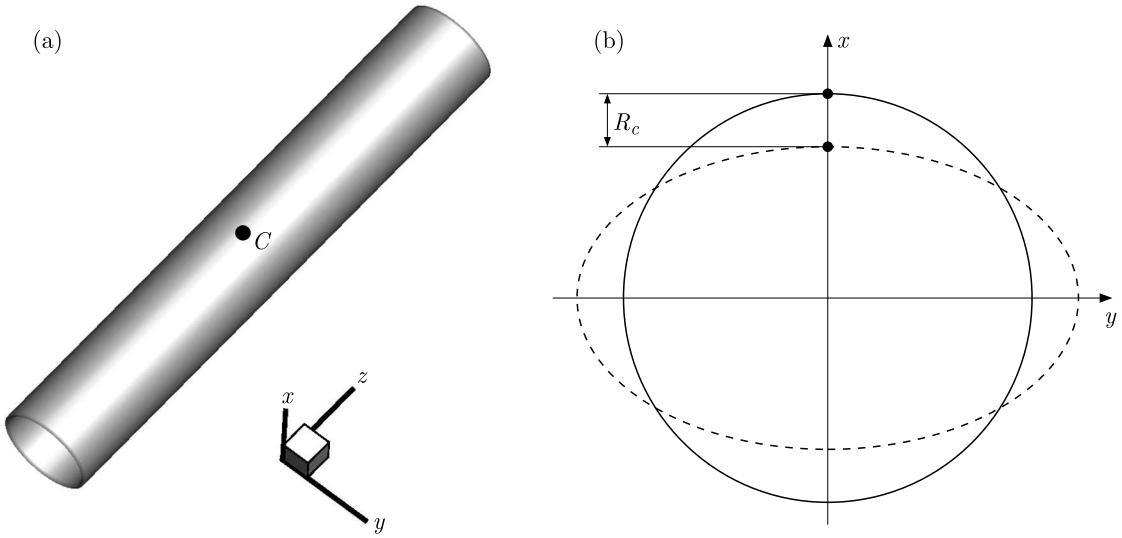

Fig. 7. The displacement of point C in the perturbation direction: (a) position of point C, (b) magnitude of displacement

The initial conditions of the transient solution are obtained by perturbing the external pressure of the steady solution. In the specific implementation, the displacement of point C on the disturbed tube, and the steady solution after the disturbance is calculated by the displacement control method as the initial gauss of the transient solution. In this way, one can avoid a too large external pressure disturbance, which leads to too large deformation of the tube and does not meet the conditions as the initial gauss of the transient solution. Point C is located at the middle of the tube collapsible section, and its coordinates are $(x = R+h, y = 0, z = L_u+0.5L_m)$, as shown in Fig. 7a. The point C is disturbed in the x direction and its displacement is R_c, as

shown in Fig. 7b. The solid line and dotted line represent the shape of the cross section at point C before and after deformation, respectively.

We will solving the transient solution of the system in three different conditions. In the first condition, Re is 150 and the external pressure P^*_{ext} is changed from 19.48 Pa to 19.49 Pa when the displacement of point C in the perturbation direction R_c is disturbed from -0.15 to -0.1625. In seeking the transient solution of the system, we set the external pressure $P^*_{ext} = 19.48$ Pa and take the steady solution of the system when $P^*_{ext} = 19.49$ Pa as the initial condition of the transient solution. In the steady buckling solution under external pressure $P^*_{ext} = 19.48$ Pa, the coordinate of point C is $(x = 0.37500, y = 0.00000, z = 5.50021)$ whose abscissa is shown by the red line in Fig. 8a. The black line in Fig. 8a shows the time varying curve of the abscissa of point C in the transient solution. It can be seen that the abscissa of point C vibrates with the position of the steady solution as the balance point. Since the energy entering the system is less than the energy dissipated in the flow field, the amplitude of vibration gradually decreases. The amplitude of the first cycle is 0.01220 and the amplitude of the last cycle is 0.00110, which is less than one tenth of that of the first cycle. It can be inferred that as time goes on, the abscissa of point C will tend to the abscissa value of the steady solution when the external pressure $P^*_{ext} = 19.48$ Pa, that is, 0.37500. Therefore, the steady solution is stable under this parameter, which is consistent with the conclusion obtained by solving the eigenvalue of the stability problem of the steady solution in Section 4.2.

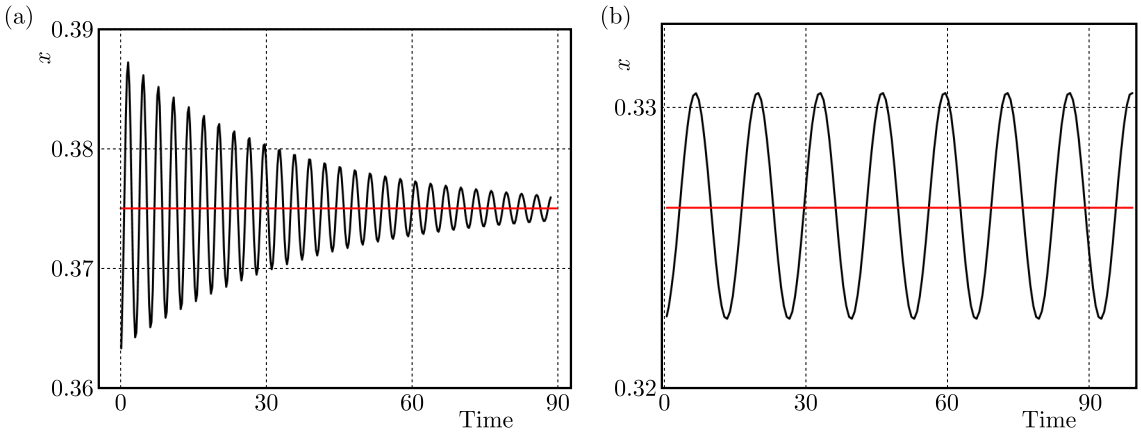

Fig. 8. The time-dependent curves of x coordinate of point C in the pressure driven condition when $P^*_{ext} = 19.48$ Pa as described by the black lines, and the red lines show the x coordinate of point C in the steady buckling solution: (a) Re = 150, (b) Re = 200

In the second condition, Re is 200 and the external pressure P^*_{ext} is changed from 19.48 Pa to 19.49 Pa when the displacement of point C in the perturbation direction R_c is disturbed from -0.198 to -0.2020. In seeking the transient solution of the system, we set the external pressure $P^*_{ext} = 19.48$ Pa and take the steady solution of the system when $P^*_{ext} = 19.49$ Pa as the initial condition of the transient solution. The black line in Fig. 8b shows the change of the abscissa of the point C of the transient solution when $P^*_{ext} = 19.48$ Pa where the red line ($x = 0.32700$) is the abscissa of the point C of the steady solution. It can be seen that the abscissa of point C vibrates with the red line and the amplitude remains unchanged over time. The system is in a critical state between stable and unstable, which is consistent with the conclusion obtained by solving the eigenvalue of the stability problem of the steady solution in Section 4.2.

In the third condition, Re is 200 and the displacement of point C is perturbed from -0.172 to -0.179 where the external pressure is changed from $P^*_{ext} = 19.36$ Pa to $P^*_{ext} = 19.39$ Pa. Take the steady solution under $P^*_{ext} = 19.39$ Pa as the initial guess to solve the transmit solution under $P^*_{ext} = 19.36$ Pa. As shown in Fig. 9, the black line in the figure is a time varying curve

of the abscissa of point C in the transient solution, and the red line ($x = 0.353$) is the abscissa of point C in the steady solution. The abscissa of point C vibrates with the red line and the amplitude is increasing with time. So, the steady solution is unstable and the conclusion is also the same as that in Section 4.2.

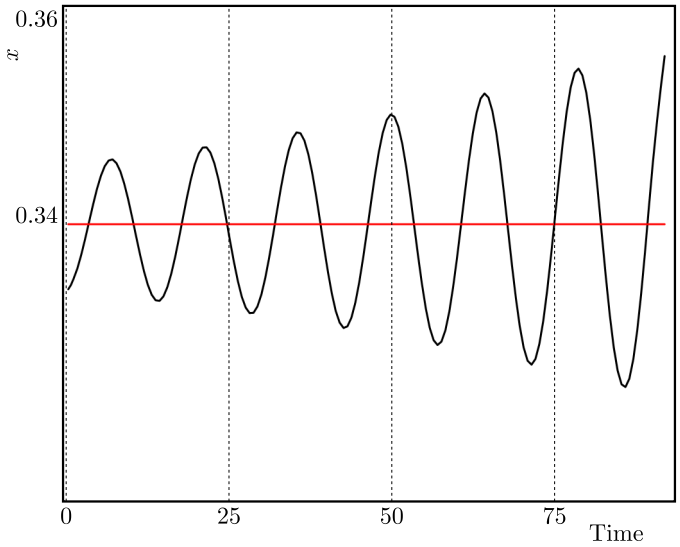

Fig. 9. The time-dependent curve of x coordinate of point C in the pressure driven condition when $P^*_{ext} = 19.36\,\mathrm{Pa}$, $\mathrm{Re} = 200$ as described by the black line, and the red line shows the x coordinate of point C in the steady buckling solution

It can been seen that determining stability of the steady solution by solving the transient solution derives the same conclusion with the eigenvalue method. In practical calculation, the time consumed by solving the transient solution is ten or tens times more than that in the eigenvalue method. It shows the effectiveness of the eigenvalue method.

5. Conclusion

We have carried out an extensive study on three-dimensional flows in a hyper-elastic collapsible tube in a pressure-driven condition. The rotating spines method is developed to solve the coupled fluid structure interaction problem when the tube is greatly collapsed. We found that there exists a range of Reynolds numbers when two solutions exist at the same external pressure, with one non-buckling and one buckling scenarios (Fig. 6b). This type of bifurcation diagrams for the tube buckling has not been reported before and it is very different to that in the flow-driven boundary condition (Truong and Bertram, 2009). It is the first time to determine stability of the steady solution by the eigenvalue method and the solution may be stable, unstable or in a critical state between stable and unstable in some range of Reynolds numbers. The transient solutions of the system are obtained to validate the effectiveness of the eigenvalue method to determine stability of the steady solution. By changing the core parameters of the system (Reynolds number and elastic modulus of the tube), the stability parameter space of the system with respect to the Reynolds number and elastic modulus can be determined. Analysis of the rule between system stability and its parameters, one can provide a reference for stugy of the mechanism of self--excited vibration. It also provides theoretical support for design and manufacture of auxiliary vocal devices and snoring control equipment.

Acknowledgments

This work was supported by national key research and development program (No. 2021YFB2401700) and Guangdong key research and development program (grant No. 2021B0101190001).

References

1. Bertram C.D., 2003, *Experimental studies of collapsible tubes*, [In:] *Flow Past Highly Compliant Boundaries and in Collapsible Tubes. Fluid Mechanics and Its Applications*, P.W. Carpenter, T.J. Pedley (Edit.) , **72**, 51-65, Springer, Dordrecht
2. Bertram C.D., Truong N.K., Hall S.D., 2008, PIV measurements of the flow field just downstream of an oscillating collapsible tube, *Journal of Biomechanical Engineering*, **130**, 6, 061011
3. Gresho P.M., Lee R.L., Sani R.L., 1980, On the time-dependent solution of the incompressible Navier-Stokes equations in two and three dimensions, *Recent Advances in Numerical Methods in Fluids*, **35**, 4, 205-209
4. Grotberg J.B., Jensen O.E., 2004, Biofluid mechanics in flexible tubes, *Annual Review of Fluid Mechanics*, **36**, 1, 121-147
5. Hao Y.Y., Cai Z.X., Roper S., Luo X.Y., 2016, An Arnoldi-frontal approach for the stability analysis of flows in a collapsible channel, *International Journal of Applied Mechanics*, **8**, 6, 17-29
6. Heil M., Boyle J., 2010, Self-excited oscillations in three-dimensional collapsible tubes: Simulating their onset and large-amplitude oscillations, *Journal of Fluid Mechanics*, **652**, 405-426
7. Heil M., Jensen O.E., 2003, Flows in deformable tubes and channels theoretical models and biological applications, [In:] *Flow Past Highly Compliant Boundaries and in Collapsible Tubes. Fluid Mechanics and Its Applications*, P.W. Carpenter, T.J. Pedley (Edit.) , **72**, 15-49, Springer, Dordrecht
8. Jensen O.E., Heil M., 2003, High-frequency self-excited oscillations in a collapsible-channel flow, *Journal of Fluid Mechanics*, **481**, 235-268
9. Liu H.F., Luo X.Y., Cai, Z.X., 2012, Stability and energy budget of pressure-driven collapsible channel flows, *Journal of Fluid Mechanics*, **705**, 348-370
10. Luo X.Y., Cai Z.X., Li W.G., Pedley T.J., 2008, The cascade structure of linear instability in collapsible channel flows, *Journal of Fluid Mechanics*, **600**, 45-76
11. Truong N.K., Bertram C.D., 2009, The flow field downstream of a collapsible tube during oscillation onset, *International Journal for Numerical Methods in Biomedical Engineering*, **25**, 5, 405-428
12. Whittaker R.J., Heil M., Jensen O.E., Waters S.L., 2010, Predicting the onset of high--frequency self-excited oscillations in elastic-walled tubes, *Proceedings of the Royal Society A: Mathematical, Physical and Engineering Sciences*, **466**, 3635-3657
13. Yiasemides D., Argyris A., Mathioulakis D.S., 2017, Transitory and periodic flow in a self--oscillating collapsible tube: Experimental study, *Journal of Energy Engineering*, **143**, 4, 04017001
14. Zhang S., Luo X.Y., Cai Z.X., 2018, Three-dimensional flows in a hyper-elastic vessel under external pressure, *Biomechanics and Modeling in Mechanobiology*, **17**, 1187-1207

Manuscript received November 7, 2022; accepted for print January 16, 2023